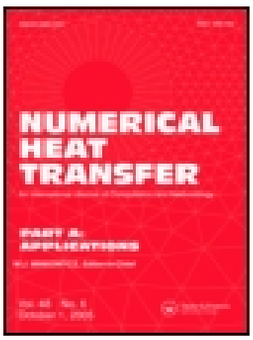

Numerical Heat Transfer, Part A: Applications

ISSN: 1040-7782 (Print) 1521-0634 (Online) Journal homepage: http://www.tandfonline.com/loi/unht20

NUMERICAL ANALYSIS IN INTERRUPTED CUTTING TOOL TEMPERATURES

Tien-Chien Jen, Gustavo Gutierrez, Sunil Eapen

To cite this article: Tien-Chien Jen, Gustavo Gutierrez, Sunil Eapen (2001) NUMERICAL ANALYSIS IN INTERRUPTED CUTTING TOOL TEMPERATURES, Numerical Heat Transfer, Part A: Applications, 39:1, 1-20, DOI: 10.1080/10407780117053

To link to this article: http://dx.doi.org/10.1080/10407780117053

Published online: 29 Oct 2010.

Numerical Heat Transfer, Part A, 39:1–20, 2001

1040-7782/01 $12.00 + .00

NUMERICAL ANALYSIS IN INTERRUPTED CUTTING TOOL TEMPERATURES

Tien-Chien Jen, Gustavo Gutierrez, and Sunil Eapen
Mechanical Engineering Department, University of Wisconsin, Milwaukee, Wisconsin, USA

A full three-dimensional numerical analysis, using a control volume approach, is conducted to study the interrupted cutting tool temperatures with temperature dependent thermal properties. The extremely small size of the heat input zone (tool-chip interface), relative to the tool insert rake surface area, requires the mesh to be dense enough to obtain accurate solutions. This usually requires very intensive computational efforts. An efficient numerical scheme is chosen to significantly reduce the required computing time. The effect of two different heat flux input profiles, a uniform heat flux and a parabolic heat flux, on the tool temperatures also are investigated.

INTRODUCTION

In any cutting process, plastic deformation involved in chip formation and friction between the tool and the workpiece produces heat by the conversion of mechanical energy. A portion of this heat conducts into the tool and results in high temperatures near the cutting edge. As the temperature increases, the tool becomes softer and wears more rapidly, thus having a negative impact on tool life. In many cutting processes, tool life, or tool wear, is the major limitation to the process viability. Increased temperature also affects the dimensional accuracy of the products and machining efficiency. Because of these considerations, it is crucial to be able to predict accurately the tool temperature.

Cutting temperatures have been studied widely for a number of years. Most research, however, has been restricted to steady state temperatures in relatively simple processes, such as orthogonal cutting or cylindrical turning, in which the cutting speed, feed rate, and the depth of cut are constant [1–3, 17, 21, 24]. In most industrial machining processes, however, these parameters vary with time so that a steady state temperature assumption may not be valid.

Received 19 June 2000; accepted 16 August 2000.

Dr. Tien-Chien Jen, Mr. Gustavo Gutierrez, and Mr. Sunil Eapen would like to thank the National Science Foundation (grant no. NSF-GOALI DMII-9908324), General Motors, the University of Wisconsin (UW System Applied Research Award), and the Society of Manufacturing Engineers (Research Initiation Award) for their financial support of the project. Acknowledgment also is made to Dr. Stanley Chen for his assistance in proofreading.

Address correspondence to Dr. T.-C. Jen, Mechanical Engineering Department, University of Wisconsin, Milwaukee, WI 53211, USA.

NOMENCLATURE

C_p	heat capacity	T	temperatures
CV	control volume	T_0	ambient temperature
CS	control surface	T_{NB}	neighbor node temperature (NB=E, W, N, S, T, B denotes east, west, north, south, top, bottom)
E_x, E_y, E_z	expansion coefficients in the x, y, and z directions	V	volume
d	tool insert dimension in the x drection	x, y, z	Cartesian coordinates
e	tool insert dimension in the y direction	$[A]$	matrix of the coefficient
f	tool insert dimension in the z direction	$\{T\}$	vector of the unknown temperature
k	tool thermal conductivity	$\{Q\}$	vector computed from the rightside of Eq. (23)
L_x	tool-chip contact length in the x direction	α_T	tool thermal diffusivity
L_y	tool-chip contact length in the y direction	$\delta(z)$	Dirac delta function
$q''(t)$	spatially uniform heat flux entering the tool	ρ	density
q''_{var}	spatially nonuniform heat flux entering the tool	θ	weighted factor in the time integration
t	time		

Recently, transient cutting tool temperatures have been investigated by various researchers [8, 16, 19, 20]. In [16] and [19], they studied the temperature distributions in interrupted cutting, a process in which the cutting speed, depth of cut, and feed rate remain constant, but in which the tool periodically enters and exits the workpiece. Both analytical models agreed reasonably well with experimental data except perhaps at a shorter cutting time interval [19]. Because of the analytical nature of the above studies, constant thermal properties were assumed to obtain the solutions. Stephenson et al. [20] and Jen and Anagonye [8] included the effects of variable thermal properties by updating the thermal properties either by using the approximate temperatures in the cutting zone or through the iteration process to update the thermal properties locally. However, in these studies, the property values for the tool insert were evaluated at the averaged temperature of the tool-chip interface. This simplification is acceptable when the thermal properties of tool insert material do not depend strongly on temperature, such as for tungsten carbide (WC). However, when the tool material thermal properties are a strong function of temperature, as is the case for high-speed steel, this effect becomes very significant [10].

Finite element methods have been used to analyze machining cutting operation and to predict cutting zone temperatures. Tay et al. [22] considered a two-dimensional case under a steady state condition, taking the thermal properties as a function of the temperature. More recently, Maekawa et al. [14] developed a finite element model to investigate the thermal behaviors in cutting processes. They studied two-dimensional cutting processes, using the thermal properties at ambient

temperature for the tool material. A multizone finite element model was used in [9] to simplify the nonlinear heat conduction equation by solving the linearized heat conduction equation in each zone. They found that the effect of variable thermal properties is very strong in materials such as high-speed steel, where thermal properties strongly depend on the temperature.

A numerical analysis, using a control volume approach, is conducted to study the interrupted cutting tool temperatures with temperature dependent thermal properties. The interrupted cutting process is highly transient because of the way the tool periodically engages and disengages the workpiece. With temperature dependent thermal properties, the governing conduction equation is nonlinear and, thus, the standard analytical solutions are no longer valid. In any cutting processes, the temperature distribution is intrinsically three dimensional, and a very steep temperature gradient may be generated in the vicinity of the tool-chip interface. In this region, where the maximum temperature occurs, the effect of variable thermal properties may become important. The full three-dimensional nonlinear transient heat conduction equation is solved numerically to study this nonlinear effect on cutting tool temperatures. The extremely small size of the heat input zone (tool-chip interface), relative to the tool insert rake surface area, requires the mesh to be dense enough to obtain accurate solutions. This usually requires very intensive computational efforts. An efficient numerical scheme is chosen to reduce significantly the required computing time. This numerical model can be used for process development in an industrial setting. The effect of two different heat flux input profiles, a spatially uniform plane heat flux and a spatially nonuniform parabolic heat flux at the tool-chip interface, on the tool temperatures are also investigated in this study.

MATHEMATICAL FORMULATION

Consider a cutting tool with a parallelepiped tool insert cutting into the workpiece (Figure 1). Heat is generated at the tool-chip interface in the corner of the rake face of the tool insert. A portion of this heat goes into the tool. To solve for the tool temperature distribution, the computational domain must be selected and appropriate boundary conditions specified. As the cutting process progresses, the heat entering the tool through the tool-chip interface penetrates further into the tool.

Ideally, the computational domain should be chosen to be larger than the depth to which there is significant heat penetration. However, this depth is not known a priori. Furthermore, if the computational domain is chosen to be larger than the tool insert, then the thermal contact resistance at the tool-holder interface must be known to specify the problem completely. Unfortunately, typically the thermal contact resistance is not known to any precision, and it depends on the particulars of the surface roughness of the interfaces and how the insert is clamped into the holder. A similar approach as in [20] can be adopted here. That is, the computational domain is selected to be the same size as the tool insert, and approximate boundary conditions are specified at the tool-holder interface, namely, ambient temperature and insulated boundary conditions, as described below.

The tool insert has three "interior boundaries" [20] in contact with the tool holder (at $x = d$, $y = e$, and $z = f$). In the approach in [20], two types of thermal

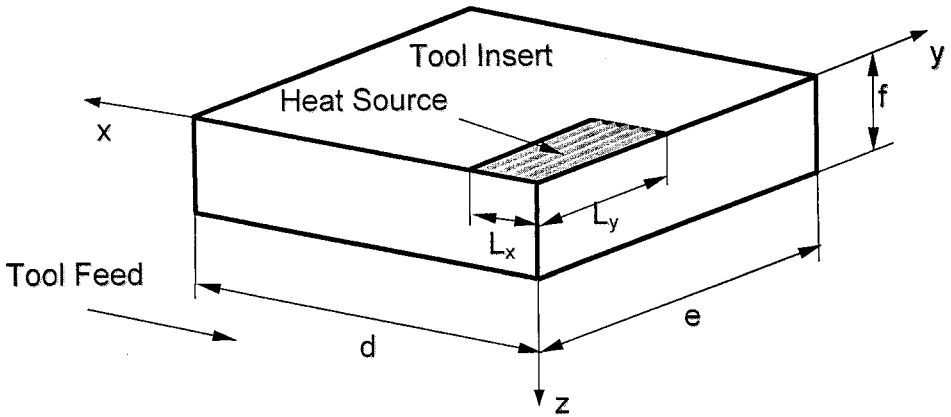

Figure 1. Geometry configuration.

boundary condition at the bottom surface of the insert ($z=f$, see Figure 1) were considered to bound the actual situation: (a) ambient temperature and (b) insulated surface. It is expected that the insulated boundary condition will yield higher calculated temperature than the ambient temperature boundary condition. It was demonstrated in their paper that the actual (measured) temperature falls between the temperature calculated for these two cases, and it is closer to the ambient temperature case than the insulated case. Based on this experimental evidence, the ambient temperature boundary condition will be used throughout this study. For the other two interior boundaries (these are farther from the heat source), only the ambient temperature boundary condition was used.

The other three "exterior" boundaries of the tool insert (at $x=0$, $y=0$, and $z=0$) are considered insulated (except where the tool is in contact with the chip). In most production processes, a water-based coolant is used to lubricate and to remove the heat from the cutting zone. It was shown in [11] that the convection effect is very significant when a water-based cutting fluid is used. It was also shown that the convection effect is relatively insignificant if no coolant is used. In this study, for simplicity, we assume the cutting operations occur under the no-coolant condition.

Given the above information, the problem can now be formulated as follows. The three-dimensional, transient heat conduction equation is

$$\rho C_p \frac{\partial T}{\partial t} = \frac{\partial}{\partial x}\left(k\frac{\partial T}{\partial x}\right) + \frac{\partial}{\partial y}\left(k\frac{\partial T}{\partial y}\right) + \frac{\partial}{\partial z}\left(k\frac{\partial T}{\partial z}\right) + q(x,y,z,t) \tag{1}$$

where t is the time, k is the thermal conductivity, ρ is the density, and C_p is the heat capacity of tool insert. The heat source term, $q(x,y,z,t)$, will be treated as a plane heat source on the surface of the insert, expressed as follows:

$$q(x,y,z,t) = \begin{cases} q''(x,y,t)\cdot\delta(z) & 0 \le x \le L_x \quad 0 \le y \le L_y \\ 0 & \text{otherwise} \end{cases} \tag{2}$$

Here, $q''(x, y, t)$ is the heat flux entering the tool through the darkened region in Figure 1. This heat flux, $q''(x, y, t)$, can vary with time and position on the surface of the insert (see [19] for possible heat flux distributions). In this study, the heat flux at the tool-chip interface, $q'(x, y, t)$, is modeled using two different profiles: a spatially uniform plane heat flux and a spatially nonuniform parabolic heat flux. For the case of spatially uniform distribution, $q''(x, y, t)$ is a constant in space denoted as $q''(t)$, which is uniform in space but may be varying with time. It is worth noting that the parabolic profiles used in previous analyses, such as in [4], [8], [12], and [25], are all one dimensional (i.e., the heat flux varies only in one direction). This analysis will present a general form of parabolic heat flux distribution that is more realistic and can be expressed as

$$q''_{\text{var}}(x, y, t) = q''(t)\left[C_1 + \frac{36(1 - C_1)}{L_x^2 L_y^2} x(L_x - x)y(L_x - y)\right] \tag{3}$$

where C_1 is a factor varying from zero to one. For C_1 equal to zero, the heat flux input profile is fully parabolic with the heat input at the edges of the heat zone zero, and for C_1 equal to one, the heat flux will be uniform in the heat zone. For C_1 between zero and one, the heat flux distribution will be a combination of a uniform heat flux, $C_1 \times q''(t)$ plus a parabolic distribution (see Figure 2). $q''_{\text{var}}(x, y, t)$ is defined in such a way that the integration over the tool-chip interface will give the same total energy input as the case with constant heat flux.

The initial and boundary conditions are

$$T(x, y, z, 0) = T_0 \tag{4}$$

$$\left.\frac{\partial T}{\partial x}\right|_{x=0} = \left.\frac{\partial T}{\partial y}\right|_{y=0} = \left.\frac{\partial T}{\partial z}\right|_{z=0} = 0 \tag{5}$$

and

$$T(d, y, z, t) = T(x, e, z, t) = T(x, y, f, t) = T_0 \tag{6}$$

If the thermal properties are constants, Eq. (1) becomes

$$\frac{1}{\alpha_T}\frac{\partial T}{\partial t} = \frac{\partial^2}{\partial x^2} + \frac{\partial^2 T}{\partial y^2} + \frac{\partial^2 T}{\partial z^2} + \frac{q(x, y, z, t)}{k_T} \tag{7}$$

where α_T is the tool thermal diffusivity. Since the thermal properties are constant, Eq. (7) is a linear partial differential equation that can be solved analytically, provided the boundary conditions, tool geometry, and heat input functions are simple enough, as in [20]. Two different materials are used as cutting tool materials: high-speed steel and WC. These materials are commonly used in the machining industry. The thermal properties for the high-speed steel are obtained from [7] and correlations were listed in Eqs. (8)–(11). For the high-speed steel,

$$k_T(\text{W/m°C}) = -0.047T(\text{°C}) + 61.16 \tag{8}$$

$$C_P(\text{J/kg°C}) = 0.0019T(\text{°C})^2 - 0.55T(\text{°C}) + 478.5 \tag{9}$$

For the WC tool material, a correlation for temperature dependent thermal proper-

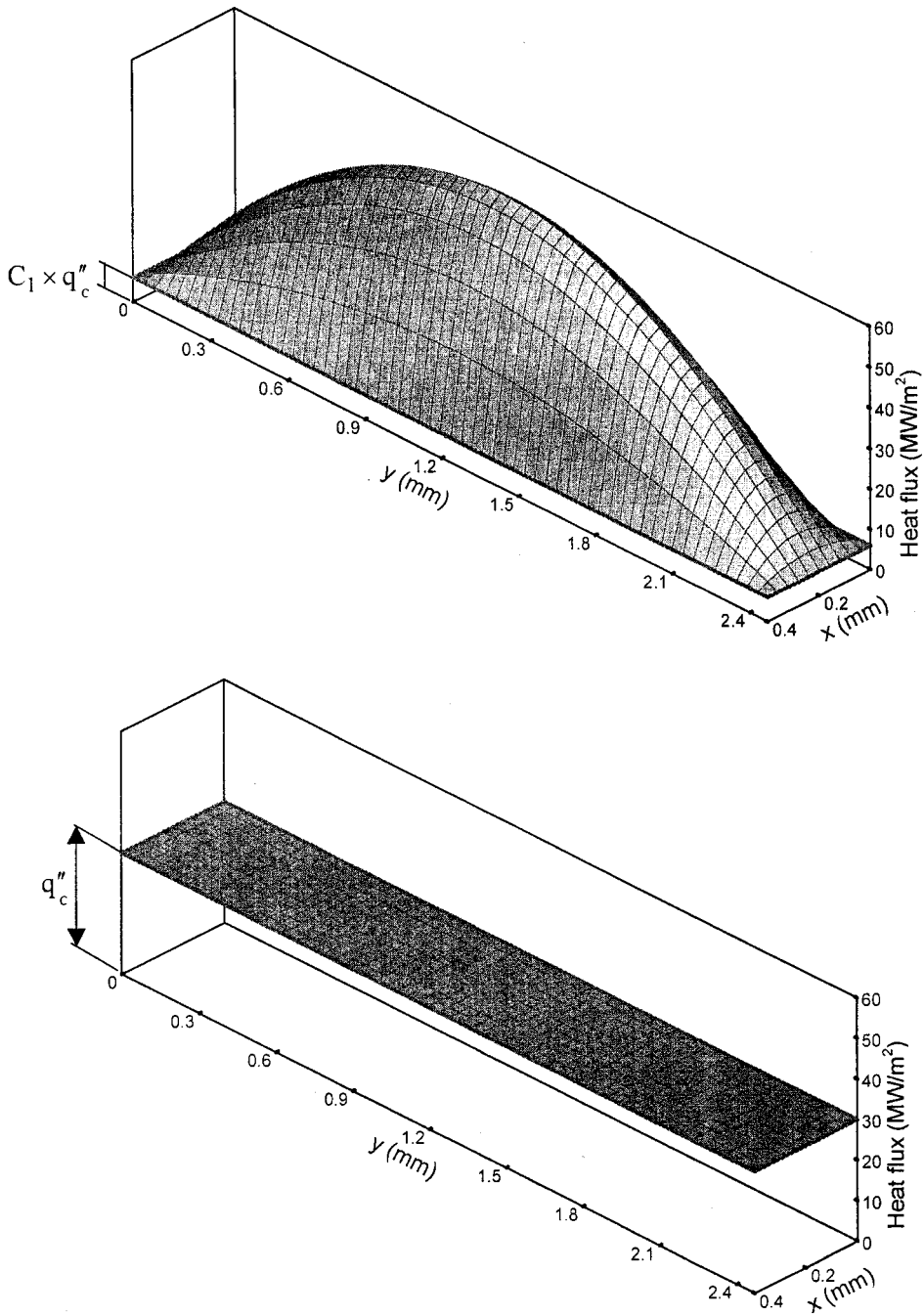

Figure 2. Heat flux input profiles.

ties developed by [18] was used. For the WC,

$$k_T(\mathrm{W/m^\circ C}) = 0.0099T(^\circ\mathrm{C}) + 57.7 \tag{10}$$

$$C_P(\mathrm{J/kg^\circ C}) = 0.435T(^\circ\mathrm{C}) + 443.7 \tag{11}$$

These correlations show that the conductivity k_T for high-speed steel decreases with temperature, whereas the behavior for WC (Sandvik S-2) is the opposite. It can be seen from Eqs. (8)–(11) that the thermal property of high-speed steel has much stronger temperature dependence than WC. In this study, the consequences of this difference in thermal properties behavior is investigated numerically.

NUMERICAL MODELING

To account for the nonlinearities because of the temperature dependent thermal properties, a numerical code was developed to solve the governing equation. The full nonlinear heat conduction equation (i.e., Eq. (1)) is discretized using a control volume approach ([15] and [27]). In this method, the equation is integrated over each control volume and for a transient analysis over each time step such as

$$\int_t^{t+\Delta t}\int_{CV}\rho C_p\frac{\partial T}{\partial t}dV\,dt = \int_t^{t+\Delta t}\int_{CV}\frac{\partial}{\partial x_i}\left(k\frac{\partial T}{\partial x_i}\right)dV\,dt + \int_t^{t+\Delta t}\int_{CS} q(x,y,t)dS\,dt \tag{12}$$

The last term in the right-hand side is only nonzero at the chip interface where the heat flux is imposed. If the temperature at the node is assumed to prevail over the whole control volume, the left-hand side can be written, using a first-order (backward) differencing scheme, as

$$\int_{CV}\int_t^{t+\Delta t}\rho C_p\frac{\partial T}{\partial t}dt\,dV = \rho(C_pT_P - C_P^0T_P^0)\Delta V \tag{13}$$

where the superscript "o" refers to temperature at time t and temperatures at time $t+\Delta t$ are not superscripted. For the diffusion term on the right-hand side central differencing is used. The x direction yields

$$\begin{aligned}\int_t^{t+\Delta t}\int_{CV}\frac{\partial}{\partial x}\left(k\frac{\partial T}{\partial x}\right)dV\,dt &= \int_t^{t+\Delta t}\left[\left(kA\frac{\partial T}{\partial x}\right)_e - \left(kA\frac{\partial T}{\partial x}\right)_w\right]dt \\ &= \int_t^{t+\Delta t}\left[k_eA_e\frac{T_E-T_P}{\delta_{EP}} - k_wA_w\frac{T_P-T_W}{\delta_{PW}}\right]dt \\ &= \int_t^{t+\Delta t}[a_eT_E + a_wT_W - (a_e+a_w)T_P]dt\end{aligned} \tag{14}$$

where $a_e = k_eA_e/\delta_{EP}$ and $a_w = k_wA_w/\delta_{PW}$. Performing the same analysis for the y and z directions, we can write the diffusion term as

$$\int_t^{t+\Delta t}\int_{CV}\frac{\partial}{\partial x_i}\left(k\frac{\partial T}{\partial x_i}\right)dV\,dt = \int_t^{t+\Delta t}\left(\sum_{NB}a_{NB}T_{NB} + a_PT_P\right)dt \tag{15}$$

where the subscript "NB" denotes neighbor value. The coefficients a_{NB} have the form

$$a_{NB} = \frac{k_{NB} A_{NB}}{\delta_{NB}} \qquad \text{for } NB = E, W, N, S, T, B \tag{16}$$

where E, W, N, S, T, and B denote east, west, north, south, top, and bottom nodes following the geographic nomenclature (see Figure 3). The coefficient a_P has the form

$$a_P = -(a_E + a_W + a_N + a_S + a_T + a_B) \tag{17}$$

For the time integration the "generalized trapezoidal rule" is used:

$$\int_t^{t+\Delta t} a_i T_i \, dt = [\theta a_i T_i + (1-\theta) a_i T_i^0] \Delta t \tag{18}$$

where the subscript "i" denotes any of the coefficients a_{NB} or a_P and the coefficient θ is a weighting factor varying from zero to one. The heat flux is integrated using the mean value

$$\int_t^{t+\Delta t} \int_{CS} q''(x, y, t) dS \, dt = \overline{q''(x, y, t)} \Delta S \, dt \tag{19}$$

where ΔS is the face area of the control volume at the chip interface. After assemb-

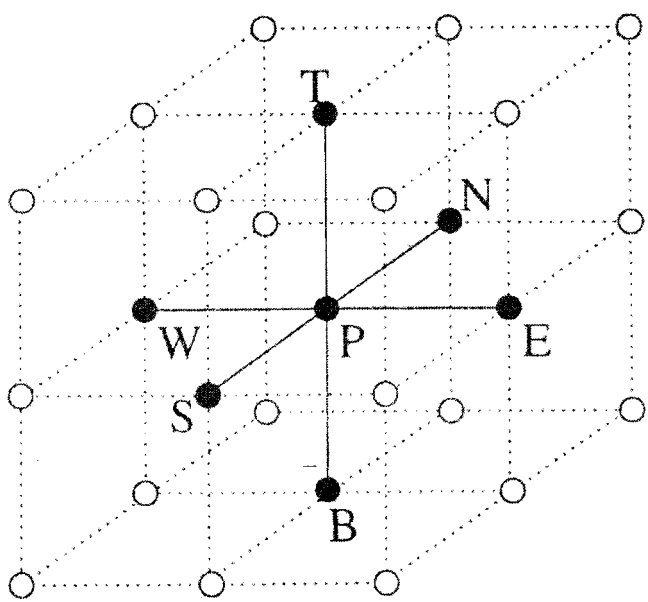

Figure 3. Nodes arrangements in three dimensions.

ling the equations for all the control volumes, we have

$$A_P T_P + \sum A_{NB} T_{NB} = A_P^0 T_P^0 + \sum A_{NB}^0 T_{NB}^0 + b \tag{20}$$

where

$$A_{NB} = \theta a_{NB}$$

$$A_P = -(a_E + a_W + a_N + a_S + a_T + a_B) - \frac{\rho C_P \Delta V}{\Delta t} \tag{21}$$

$$A_P^0 = -(\theta - 1)(a_E + a_W + a_N + a_S + a_T + a_B) - \frac{\rho C_p^0 \Delta V}{\Delta t} \tag{22}$$

and

$$b = \overline{q''(x, y, t)} \Delta S \, dt \tag{23}$$

Coefficients A_P and A_{NB} in Eq. (20) involve the properties k and C_p, which are a function of the temperature at time $t + \Delta t$. Then the problem must be solved iteratively updating the thermal properties until a convergence for each time step is obtained. Equation (20) can be written in matrix form as

$$[A]\{T\} = \{Q\} \tag{24}$$

where $[A]$ is the matrix of the coefficients, $\{T\}$ is the vector of the unknown temperatures, and $\{Q\}$ is a vector computed from the right-hand side of Eq. (20), which are all known values obtained either from the initial condition or from the previous time step. To solve the matrix system, Eq. (24), four different numerical schemes were tested: SIP3D (strongly implicit procedure in three dimensions), ICCG (conjugate gradient method, using an incomplete Cholesky decomposition), CGSTAB (conjugate gradient stabilized) proposed by Van den Vorst and Sonneveld [26] and TDMA (line-by-line using the three diagonal matrix algorithm). A complete description of these algorithms can be found in [6]. The algorithms were modified and adapted from the codes provided by [5].

The temperatures at the insulated surfaces and at the tool-chip interface are calculated using a parabola fit to the boundary and two inner points. This approximation is of second-order accuracy in space. In all that follows, unless otherwise stated, the tool dimensions used in all the computations are $d = e = 13.47$ mm and $f = 3.35$ mm and the tool interface dimensions are $L_x = 0.4$ mm and $L_y = 2.47$ mm.

Grid System

Because of the nature of the problem, the cutting zone area needs a much better resolution to achieve accurate results. An expansion coefficient in each direction is used to increase the number of nodes in the cutting region. These expansion coefficients are defined as

$$E_x = \frac{\Delta x_{I+1}}{\Delta x_I} \quad E_y = \frac{\Delta y_{J+1}}{\Delta y_J} \quad E_z = \frac{\Delta z_{K+1}}{\Delta z_K} \tag{25}$$

To keep the accuracy at second order, the expansion coefficients are chosen close to unity. In all the computations, the shape of the control volume in the cutting region is to keep as much uniform as possible with an aspect ratio near to one. The aspect ratio far away from the cutting zone is larger than one because of the small temperature gradient there. A grid refinement test is conducted to decide an adequate grid distribution. For grid independent tests, a steady state case with a constant heat flux of 30 MW/m^2 is selected. The test is performed for four different grid sizes with three sets of expansion coefficients. In all the cases, the expansion coefficients in the three directions are chosen to be the same. High-speed steel is selected for the test because the effect of the nonlinearities is stronger for this material as it is shown later. A grid of $70\times70\times16$ with an expansion coefficient of 1.04 in each direction ensures a satisfactory solution and was selected for all the computations.

Convergence Criterion

The numerical computation is considered converged when the residual summed over all the computational nodes satisfies the following criterion:

$$\text{Residual} = \sum_{i=1}^{\text{number of nodes}} (\{Q\} - [A]\{T\})_i \leq 0.005 \tag{26}$$

where $(\{Q\}-[A]\{T\})_i$ represents the residual for the node i. This is the criterion for the outer iteration. For inner iterations, the properties are updated when the residual decreases to 0.01 of the initial residual for the current values of the thermal properties. After a number of inner iterations, the solution converges to the appropriate values of the temperatures, thermal conductivity, and specific heat. A numerical test was carried out to analyze the efficiency of these algorithms. The same steady state case was run for a constant heat flux and for the high-speed steel using four numerical schemes enumerated above. Figure 4 shows the convergence history for the different numerical schemes. We can see from Figure 4 that the CGSTAB has the best performance, and it will be used for all the computations. For the TDMA method as can be seen from Figure 4, the speed of convergence is roughly about two orders of magnitudes less than the other methods. This becomes particularly important in transient analysis where the convergence has to be reached for each time step.

RESULTS AND DISCUSSION

The tool insert geometry used in this study is $d=f=13.6$ mm, and $e=3.35$ mm. Unless otherwise stated, this tool geometry will be used throughout this section.

Before proceeding to discuss the calculated results, some validation comparisons are discussed. A benchmark test for testing the present finite volume model with the analytical results has been performed. The data used for comparison were adopted from Stephenson and Ali [19] for an interrupted cutting case. Note that the single point temperature is usually more sensitive than the averaged temperature in the numerical analysis of cutting temperature. Thus, the time temperature history

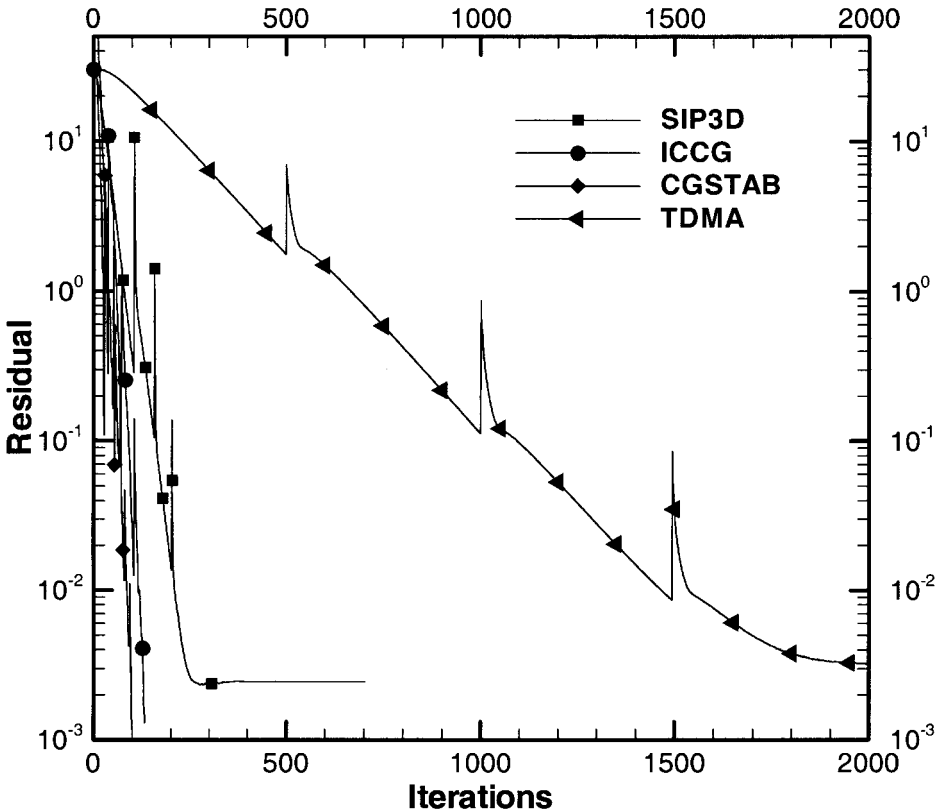

Figure 4. Convergence history for the different numerical schemes.

is compared for a point $x = L_x/2$, $y = L_y/2$, and $z = 0$. The intermittent heat flux input of $q'' = 65$ MW/m^2 (for spatially uniform distribution), and the cutting and uncut time are 0.04 s and 0.04 s, respectively. Since the analytical solution is valid only when the thermal properties are constant, it is simulated using constant thermal properties with $k = 75$ W/mK. It can be seen from the figure that the current finite volume model agrees very well with their analytical solutions as shown in Figure 5. With this agreement and the grid convergence tests shown before, we are confident that this numerical code is valid to further compute the interrupted cutting cases.

To further verify the model predictions, we compared experimental results reported in [19] for interrupted cutting cases with the current numerical model (Figures 6*a* and 6*b*). In [19], they measured the tool-chip interface temperature using a tool-workpiece thermocouple method. For the cases shown in Figures 6*a*, 6*b*, gray cast iron with a WC tool was used, with $\tau_1 = 0.0374$ (cutting time step) and $\tau_2 = 0.0067$ (cooling time step) in Figure 6*a*, and with $\tau_1 = 0.0183$ and $\tau_2 = 0.0248$ in Figure 6*b*. It can be seen from Figure 6*a* that the current numerical model predicts

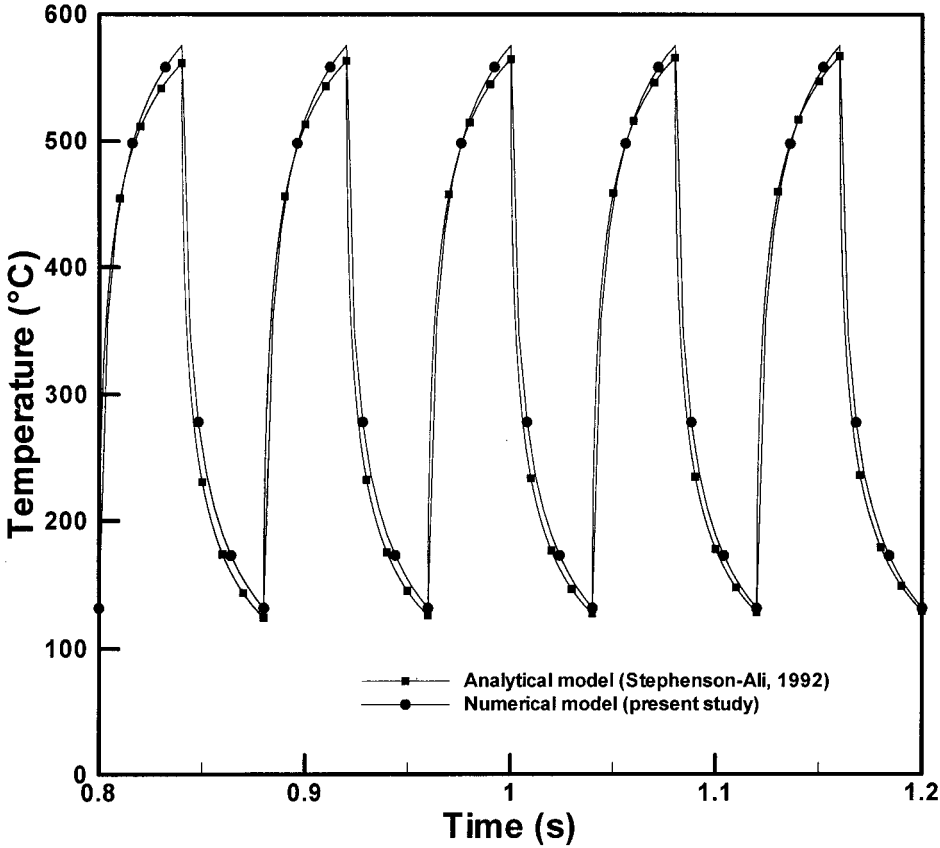

Figure 5. Benchmark test.

Table 1 Grid independent rest (temperature at the corner is selected as a test parameter)

	Grid (I,J,K)			
Exp. coeff.	40×40×10 (16,000 nodes)	50×50×12 (30,000 nodes)	70×70×16 (78,400 nodes)	80×80×20 (128,000 nodes)
1.03	506	503	499	497
1.04	500	502	498	497
1.05	506	498	497	496

Figure 6*a*

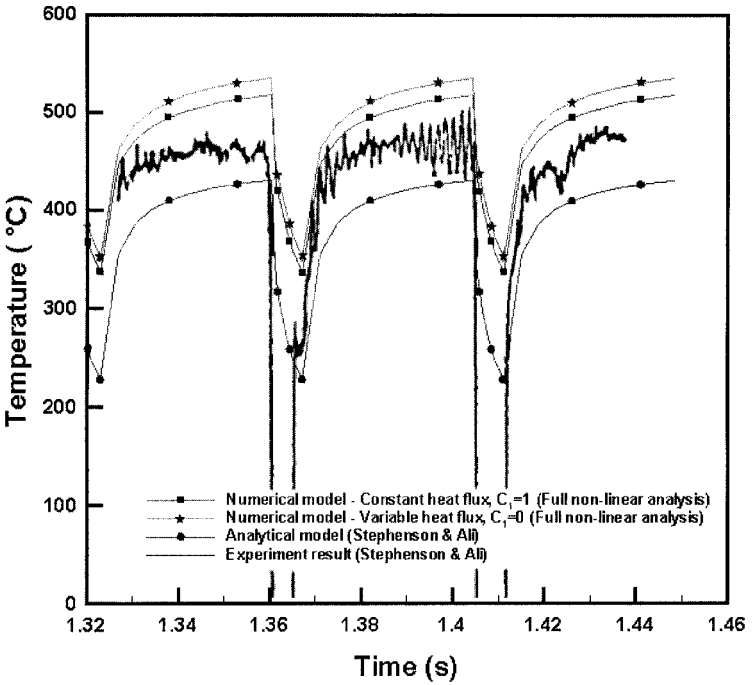

Figure 6*b*

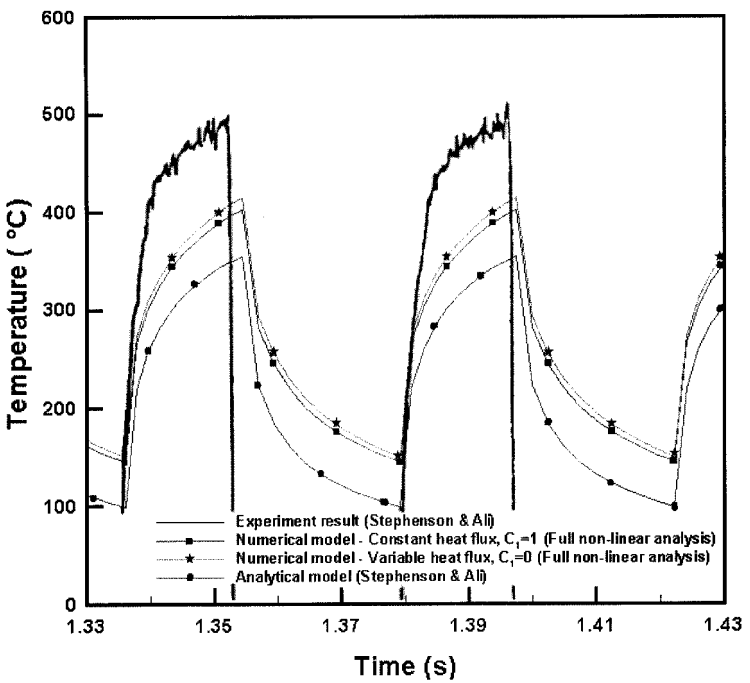

Figure 6. Comparison with experimental results.

the tool-chip interface temperature slightly higher than the experimental results, while the analytical results in [19] fell lower than the experimental data. For the two curves shown in this study, one is for the case of uniform heat flux input (i.e., $C_1 = 1$) and the other is for the case with parabolic heat flux input (i.e., $C = 0.0$). The difference of the averaged tool-chip interface temperature for the different heat flux input profiles is small, about 10°C in this case.

Figure 6*b* shows the cases with a larger uncut time period, i.e., $\tau_2 > \tau_1$. In this case, the analytical data by [19] agree poorly with the experimental data. With the consideration of temperature dependent thermal properties, the current numerical results show better agreement with the experimental data. However, the error is still fairly significant, about 20% in temperature prediction. One possible reason for this discrepancy is that the energy partitioning is highly transient, whereas the study in [19] calculated the energy partition using a quasi-steady approach [13]. Very recently, Jen and Anagonye [8] developed a transient energy partition model by modifying Loewen and Shaw's [13] model. They showed their results agree favorably with the experimental data. However, their model shared the common drawback that the entire tool insert thermal properties were evaluated at either the ambient temperature or the updated averaged tool-chip interface temperature.

Figure 7 shows the effect of the variable thermal properties on maximum temperatures for the two different materials, namely, high-speed steel and WC. Heat fluxes on the tool-chip interface are assumed uniform, and for each material two curves representing the analytical model with thermal properties evaluated at ambient temperature and the full nonlinear numerical analysis, respectively, are shown in this figure. The horizontal coordinate is the heat flux input to the tool insert in MW/m^2 and the vertical coordinate is the maximum temperature reached for the steady state under continuous cutting conditions. In general, the temperature differences between the linear and the nonlinear cases increase for increasing heat fluxes because higher temperatures are generated. Note that the thermal conductivity decreases when the temperature is increased for the high-speed steel, whereas it increases for the WC. The much stronger effect on maximum temperatures when high-speed steel is used as the cutting tool material is no surprise. This can be seen directly from Eqs. (8) and (10). The leading coefficients for high-speed steel and WC are -0.047 and 0.0099, respectively. This reveals that there is merely a factor of 5 difference in thermal conductivity variations under the same temperature difference. If we compare the temperature differences at 30 MW/m^2 for both materials with the constant thermal property cases, the temperature differences are 84°C and 17°C for high-speed steel and WC, respectively. This exactly reflects the factor of 5 difference discussed above. Thus, a much stronger effect on temperature variations should be expected for the cutting tool made of high-speed steel. As was mentioned before, if the thermal conductivity is assumed constant, the governing equation is linear and can be solved analytically [20]. Typically, the thermal conductivity is evaluated at ambient temperature or the updated temperature at the tool-chip interface of each time step. If the conductivity is a strong function of tool temperature, the governing heat conduction equation (Eq. (1)) becomes nonlinear and a numerical analysis is required to obtain an accurate solution.

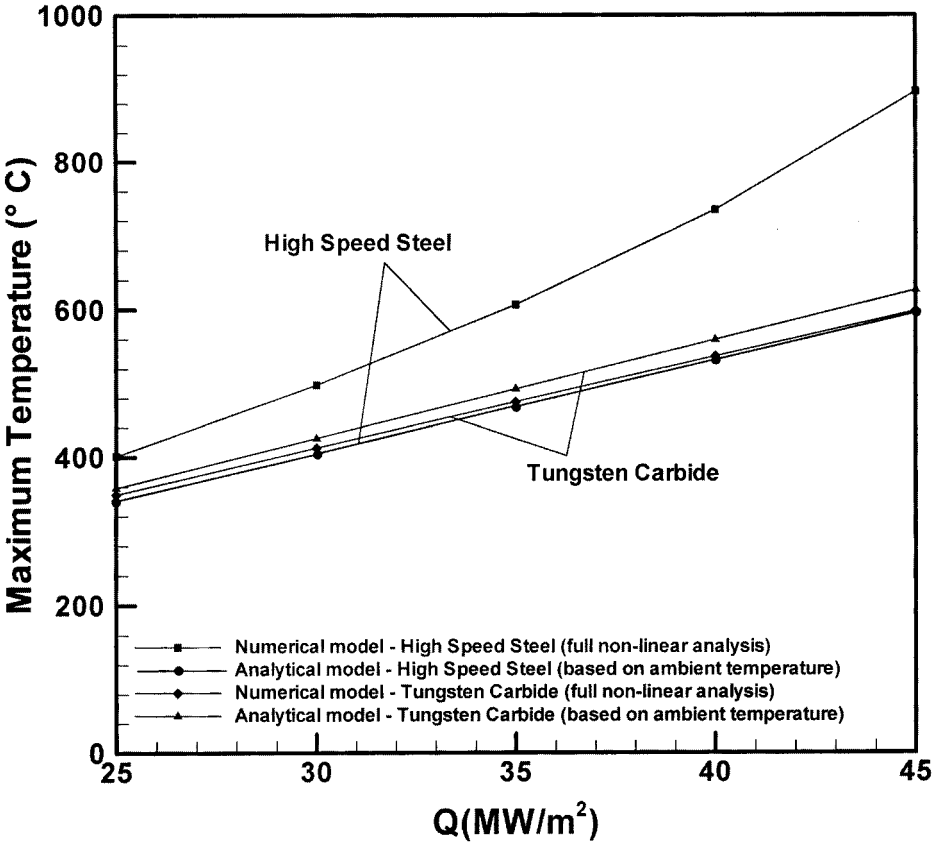

Figure 7. Effects of the variable thermal properties.

Figure 8 shows a comparison of maximum temperatures between the linear and the nonlinear cases under interrupted cutting conditions. Only high-speed steel tool material cases are depicted in this figure since this material has strongly temperature dependent thermal properties. The uniformly distributed heat flux input at the tool-chip interface is set to be 30 MW/m^2, and the cutting and uncut times are equal and set to be 0.04 seconds. It can be seen from the figure that even for a short time, the effect of the variable thermal properties is very significant, for instance at the end of the first cutting period, $t = 0.04$ seconds, the maximum temperature difference is of the order of 10%. As shown in the figure, the maximum temperature difference is as large as 14% by the time the cutting process reaches periodic steady state. As mentioned earlier, many different cutting processes, such as milling, interrupted cutting, and so on, are essentially transient because of periodic engagement and disengagement of the cutting tool to the workpiece. This study also reveals that for cutting processes that are highly transient, the effect of temperature dependent thermal properties may be significant if the thermal property of the cutting material is a strong function of temperature.

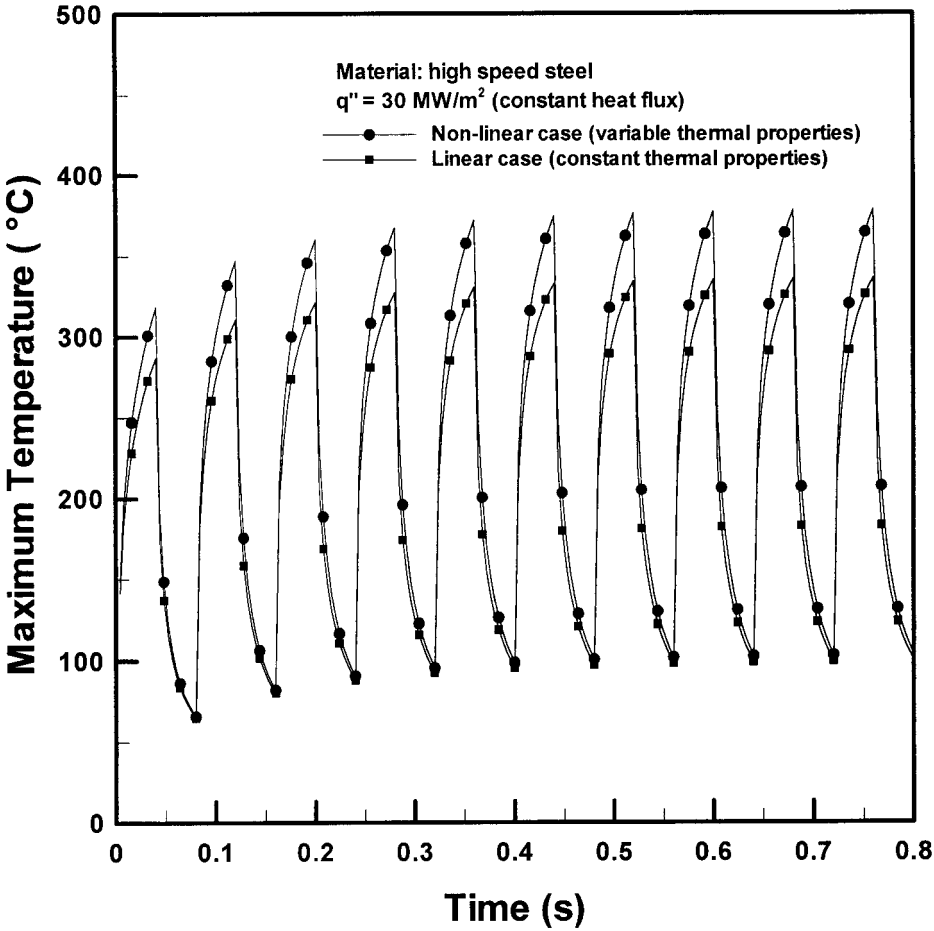

Figure 8. Effects of the variable thermal properties on maximum temperatures for interrupted cutting.

In many earlier studies, such as in [4], [8], [12], and [25], a one-dimensional heat flux distribution profile along the tool-chip interface was assumed (i.e., varies in the chip flow direction *only*). This indicates that their analyses are, strictly speaking, two dimensional. This assumption was made because of experimental evidence (see, e.g., [23]), suggesting that the maximum temperature should be located somewhere in the middle of the tool-chip interface, instead of on the tip of the cutting tool. However, in the actual cutting process, the heat flux distribution profile on the tool-chip interface as well as the tool temperature distribution are intrinsically three dimensional. Thus, a one-dimensional heat flux distribution profile on the tool-chip interface may not reflect accurately the true heat flux distribution on the tool-chip interface. This study is aiming to eliminate this deficiency in the earlier studies.

Figures 9*a* and 9*b* show the effect of different heat flux input profiles at the tool-chip interface on the maximum temperature under interrupted cutting con-

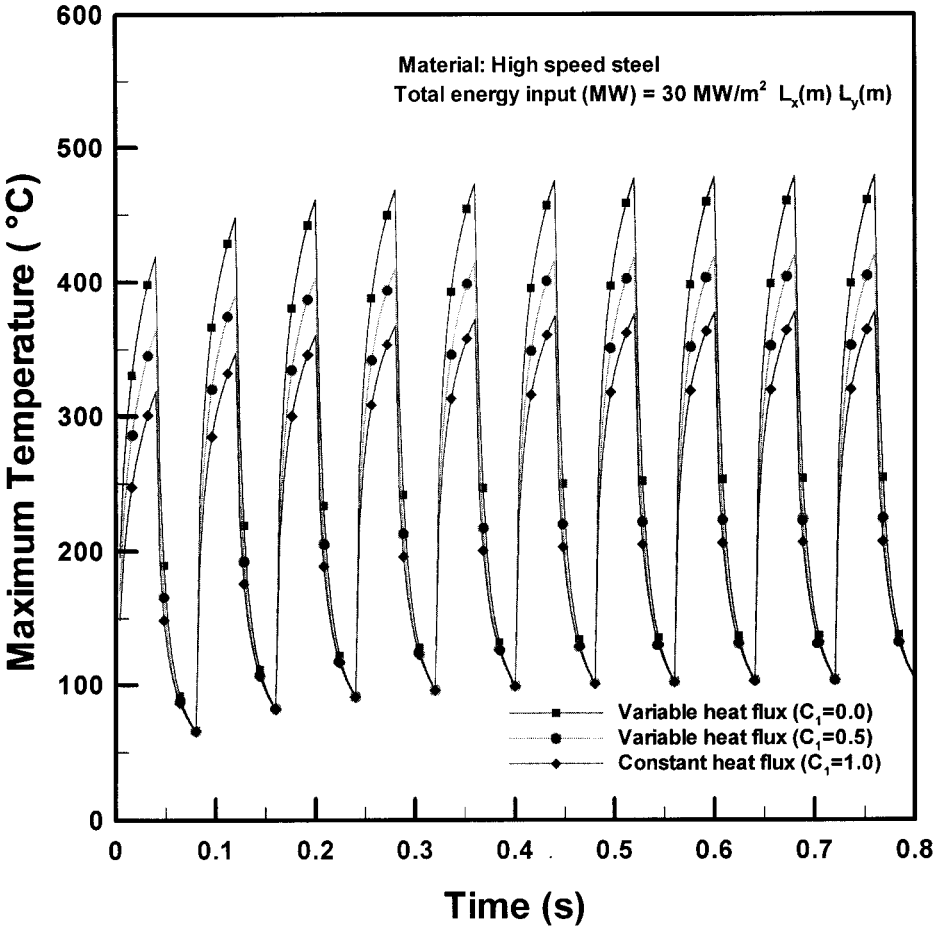

Figure 9. Effects of the heat flux input profiles on maximum temperatures for interrupted cutting.

ditions. For the purpose of simplifying comparisons, the total heat input for different heat flux input profiles is exactly identical, that is, 30 MW/m^2 for the uniform heat flux input case. A high-speed steel material is used in Figure 9*a*, and in Figure 9*b* the tool material is WC. Three different heat flux input profiles are used in the figures: $C=0.0$ (fully parabolic), $C=0.5$, and $C=1.0$ (uniform). It can be seen from the figure that there is a strong effect of different heat flux profiles on maximum temperatures at the tool-chip interface. The parabolic heat flux input profile can be thought to be more realistic than the uniform heat flux input profile because the maximum crater wear occurs somewhere in the middle section of the tool-chip interface [23]. Also, a higher temperature can be generated because of the more concentrated heat input at the center section of the tool-chip interface (see Figure 2). This may cause a more significant effect because of the temperature dependent thermal properties. In Figure 9*a*, with the high-speed steel tool material, the differ-

ence in maximum temperature for uniform heat flux input (i.e., $C = 1.0$) and the fully parabolic profile input (i.e., $C = 0.0$) is in the order of 100°C, which is more than 20% in the case shown. For the WC tool material as shown in Figure 9*b*, the difference in maximum temperature for the cases of $C = 1.0$ and $C = 0.0$ is about 70°C, which is generally less than 20%. This is no surprise since the high-speed steel has stronger temperature dependent thermal properties.

CONCLUSIONS

A numerical study has been developed to analyze the effect of temperature dependent thermal properties on interrupted cutting processes. Two typical materials, high-speed steel and WC, commonly used as tool insert materials in machining operations, have been selected in this study. A transient non-linear three-dimensional numerical analysis has been carried out for the cases with temperature dependent thermal properties. The analysis has been compared with the linear solution, where the thermal properties are constants, to show that the effect of the nonlinearities is because of the temperature dependent thermal properties on the temperature distribution of the tool insert. Under the conditions investigated, the following conclusions can be drawn:

(a) To obtain accurate results on temperature distribution in the tool insert, a good resolution of the mesh size in the took-chip interface is needed. For the numerical scheme tested, the CGSTAB scheme gave the best performance in computational efficiency. This scheme is therefore recommended for the study of various cutting processes, including interrupted cutting processes.

(b) For high-speed steel as the tool insert material, the effect of nonlinearities because of temperature dependent thermal properties on the tool temperatures is very strong. For this material, the conductivity is a strong function of the tool temperature. When the tool temperature is increased, the thermal conductivity decreases. Thus, the heat can not be diffused effectively at the same rate, contributing to even higher temperatures in the cutting tool. It is concluded that this effect is not negligible for high-speed steel. For the tungsten carbide, this effect is not so significant because the thermal properties are much less sensitive to the temperature in typical cutting conditions. In this case, the assumption of constant thermal properties may give satisfactory results.

(c) The heat flux distribution profiles on the tool-chip interface have a significant impact on the magnitude of the maximum temperature. A general parabolic heat flux input profile was introduced in this study, which is more realistic in the actual cutting operations [23], and the predicted tool-chip interface temperature under interrupted cutting conditions agrees reasonably well with the experimental data.

(d) The maximum temperature increases significantly when the heat flux distribution departs from the uniform heat flux input profile for the same amount of total energy input. Under the parabolic heat flux input profile

condition, the effect of temperature dependent thermal properties becomes even more pronounced because of the local concentration of the heat flux input.

REFERENCES

1. G. Barrow, A Review of Experimental and Theoretical Techniques for Assessing Cutting Temperatures, *CIRP Annals*, vol. 22, pp. 203–211, 1973.
2. G. Boothroyd and W. A. Knight. *Fundamentals of Machining and Machine Tools*, Chap. 3, Marcel and Dekker, New York, 1989.
3. A Chandra and C. L. Chan, Thermal Aspects of Machining: A BEM Approach, *Int. J. Solids. Struct.*, vol. 33, pp. 1657–1693, 1994.
4. B. T. Chao and K. J. Trigger, Temperature Distribution at the Tool-Chip Interface in Metal Cutting, *Transactions of the ASME*, pp. 1107–1121, 1955.
5. J. H. Ferzeiger and M. Peric, *Computational Methods for Fluid Dynamics*, Springer-Verlag, Berlin, Heidelberg, 1997.
6. G. H. Golub and C. van Loan, *Matrix Computations*, Johns Hopkins University Press, Baltimore, MD, 1990.
7. F. P. Incropera and D. P. DeWitt, *Introduction to Heat Transfer*, John Wiley & Sons, New York, 1996.
8. T. C. Jen and A. U. Anagonye, An Improved Transient Model of Tool Temperatures in Metal Cutting the ASME International Mechanical Engineering Congress and Exposition, Anaheim, CA, 1998; *ASME Journal of Manufacturing Science and Engineering* , to appear.
9. T. C. Jen and G. Gutierrez, Finite Element Analysis in Transient Tool Temperatures, presented at the National Heat Transfer Conference, Albuquerque, NM, 1999.
10. T. C. Jen and G. Gutierrez, Numerical Heat Transfer Analysis in Transient Tool Temperatures presented at the 2000 National Heat Transfer Conference, Pittsburgh, PA; *ASME Journal of Manufacturing Science and Engineering*, submitted.
11. T. C. Jen and A. S. Lavine, Prediction of Tool Temperatures in Interrupted Metal Cutting, in *Proc. of 7th International Symposium on Transport Phenomena in Manufacturing Processes*, pp. 211–216, 1994.
12. R. K. Levy, C. L. Tsai, and M. P. Groover, Analytical Investigation of the Effect of Tool Wear on the Temperature Variations in a Metal Cutting Tool, *ASME Journal of Engineering for Industry*, pp. 251–257, February 1976.
13. E. G. Loewen and M. C. Shaw, On the Analysis of Cutting Tool Temperatures, *ASME Trans.*, vol. 76, pp. 217–231, 1954.
14. K. Maekawa, Y. Nakano, and T. Kitawa, Finite Element Analysis of Thermal Behavior in Metal Machining, *Jpn, Soc. Mech. Eng.*, vol. 62, no 596, pp. 1587–1593, 1996.
15. S. V. Patankar, *Numerical Heat Transfer and Fluid Flow*, Hemisphere Washington, DC, 1980.
16. R. Radulescu and S. G. Kapoor, An Analytical Model for Prediction of Tool Temperature Fields during Continuous and Interrupted Cutting, *ASME Journal of Engineering for Industry*, vol. 116, pp. 135–143, 1994.
17. M. C. Shaw, *Metal Cutting Principles*, Chap. 12, Oxford University Press, Oxford, 1984.
18. D. A. Stephenson, Assessment of Steady-State Metal Cutting Temperature Models Based on Simultaneous Infrared and Thermocouple Data, *ASME Journal of Engineering for Industry*, vol. 113, pp. 121–128, 1991.
19. D. A. Stephenson and A. Ali, Tool Temperature in Interrupted Metal Cutting, *ASME Journal of Engineering for Industry*, vol. 115, pp. 432–437, 1992.

20. D. A. Stephenson, T. C. Jen, and A. S. Lavine, Cutting Tool Temperatures in Contour Turning: Transient Analysis and Experimental Verification, *ASME Journal of Manufacturing Science and Engineering*, vol. 119, pp. 494–501, 1997.
21. J. S. Strenkowski and K. J. Moon, Finite Element Prediction of Chip Geometry and Tool/Workpiece Temperature Distribution in Orthogonal Machining, *ASME Journal of Engineering for Industry*, vol. 112, pp. 313–318, 1990.
22. A. O. Tay, M. G. Stevenson, and G. Vahl Davis, Using the Fintie Element Method to Determine Temperature Distributions in Orthogonal Machining, *Proc. Instn. Mechanical Engineering*, vol. 118, pp. 627–638, 1973.
23. E. M. Trent, *Metal Cutting*, Chap. 5, Butterworths, London, 1997.
24. K. J. Trigger and B. T. Chao, An Analytical Evaluation of Metal Cutting Temperatures, *Transactions of the ASME*, vol. 73, pp. 57–68, 1951.
25. C. L. Tsai, *Finite Difference Solutions for the Time Dependent Temperature Distributions in Metal Cutting Tool*, M.S. thesis, Department of Mechanical Engineering and Mechanics, Lehigh University, Lehigh, PA, 1973.
26. H. A. Van der Vorst and P. Sonneveld, *CGSTAB, A More Smoothly Converging Variant of CGS*, Tech. Report 90-50, Delf University of Technology, 1990.
27. H. K. Versteeg and W. Malalasekera, *An Introduction to Computational Fluid Dynamic: The Finite Volume Method*, Logman Scientific and Technical, London, 1995.